METHODOLOGIES AND APPLICATION

Secondary load frequency control for multi-microgrids: HiL real-time simulation

Meysam Gheisarnejad[1] · Mohammad Hassan Khooban[2]

Abstract

The intermittent feature of renewable energy sources leads to the mismatch between supply and load demand on microgrids. In such circumstance, the system experiences large fluctuations, if the secondary load frequency control (LFC) mechanism is unable to compensate the mismatch. In this issue, this paper presents a well-structured combination of the fuzzy PD and cascade PI-PD controllers named FPD/PI-PD controller as a supplementary (secondary) controller for the secondary load frequency control in the islanded multi-microgrid (MMG). Additionally, two modifications to the JAYA algorithm are made to enhance the diversity of the initial population and ameliorate the global searching ability in the iterative process. Afterward, the improved JAYA algorithm, referred to as IJAYA, is employed for fine-tuning the proposed structured controller installed in areas of the studied MMG. The superiority of the proposed IJAYA is validated by comparative analysis with genetic algorithm and basic JAYA in a similar structure of the PID controller. Furthermore, it will be shown that the proposed FPD/PI-PD controller employing IJAYA provides a higher degree of stability in suppressing the responses deviations as compared with the conventional PID and FPID controller structures. Finally, the novel optimal proposed approach is validated and implemented in the hardware-in-the-loop (HIL) based on OPAL-RT to integrate the fidelity of physical simulation and the flexibility of numerical simulation.

Keywords Renewable energy sources · Microgrid · Load frequency control · JAYA algorithm

1 Introduction

The increasing concerns of the gradual reduction of fossil fuel reserves along with the environmental issues associated with their emissions, the potentials of alternative/renewable energy resources (e.g., offshore wind, fuel cells, solar, hydro- and bio-fuels) have been taken into account into the power grid. Due to the special advantages of renewable energy sources (RESs), such as high energy security, eco-friendly energy and low transmission losses, the applying of these sources has drawn much attention in energy policies (Bajpai and Dash 2012; Sa-ngawong and Ngamroo 2015; Torreglosa et al. 2015; Khooban et al. 2016b).

✉ Mohammad Hassan Khooban
kho@et.aau.dk; khooban@ieee.org

[1] Department of Electrical Engineering, Najafabad Branch, Islamic Azad University, Isfahan, Iran

[2] Department of Energy Technology, Aalborg University, Pontoppidanstraede 101, 9220 Aalborg, Denmark

A microgrid (MG), regarded as a regulated entity in the power system, is typically made up of a cluster of distributed generation (DG) microsources, low voltage sources such as energy storage system (ESS) and local loads as well as the infrastructure of their related equipment, which are locally accommodated for the profit of the customers. In normal condition, the MG is connected to the main utility grid (grid-connected mode) but in case of any interruption or fault in the utility, the MG will be isolated from the utility and continue to work autonomously as an island (standalone mode) (Chowdhury and Crossley 2009; Khalghani et al. 2016). The weather-dependent and intermittent behavior of some energy resources such as wind and solar is identified as one of the major threats in the standalone MG operation. The inevitable feature of RESs results in a fluctuating and unreliable power production and, consequently, leads to the imbalance between power generation and demand. Such imbalance in the power grid appears as frequency distraction which highly threatens the grid security. Moreover, the challenges of load frequency fluctuation problem will be intensified when the MGs are

interconnected as multi-microgrid (MMG) (Chowdhury and Asaduz-Zaman 2014; Kargarian and Rahmani 2015). To alleviate the variations of the power output for uninterrupted supply to the consumers and to facilitate the safe and stable operation, backup storage devices such as storage batteries, flywheels and ultra-capacitors must be properly planned with respect to the power consuming on the MG (Pan and Das 2015; Şerban and Marinescu 2011). Nevertheless, load frequency control (LFC) is essential to constantly monitor the grid frequency fluctuations and restore the term frequency within a tolerable range for correct performance of equipment.

To deal with the issue of secondary load frequency control in hybrid renewable energy systems, as a more recent trend, many control strategies such as intelligent control (Bevrani et al. 2012; Modirkhazeni et al. 2016; Khooban and Niknam 2015), H_∞ control theory (Goya et al. 2011), adaptive control (Khooban et al. 2016a) have been developed in the literature. In Pahasa and Ngamroo (2016), an MPC-based coordinated control of the blade pitch angles of the WTG and PHEV has been proposed for the LFC. The MPC controller is applied in order to smooth wind power production and decrease the number of required PHEVs. Authors of Pandey et al. (2014) suggested a robust controller using linear matrix inequalities for LFC problem consisting of different energy sources. It was successfully implemented in enhancing the system stability as well as suppressing grid frequency oscillation under load fluctuations and variations in a wind turbine. But, these sophisticated methodologies suffer from the requirement of expert designer that reduce their applicability. Alternatively, conventional PID controllers are widely adopted in literatures due to simplicity and model-free approach of design. Genetic algorithm (GA)-based PI/PID controllers is developed in Das et al. (2012) for frequency control of hybrid renewable energy technologies. In El-Fergany and El-Hameed (2017), social-spider optimizer (SSO) is implemented for optimal settings of PID controller to improve LFC performance in a standalone two-area microgrid system. In Mahto and Mukherjee (2016), four conventional controllers such as I, PI, ID and PID controllers are applied to an isolated wind diesel-hybrid power plant, and their gains are optimally designed employing quasi-oppositional harmony search (QOHS) algorithm.

In the LFC problem of an isolated MG, the classical strategies are capable to handle only a small range of operating system condition, while they are inefficient against the high variability of RESs and various system configurations. Recently, the combination of the terms of PID controller and fuzzy logic controller (FLC) has gained more attentions in the electrical power engineering topics. Since there is no a certain rule to decide the fuzzy parameters (e.g., scaling factors, membership function and rule base), heuristic techniques are often established as a straightforward approach

to design these parametric values (Khooban et al. 2017c; Mukherjee 2015).

The literature review undoubtedly divulges that in a regulatory structure of FLC coupled with PID terms, a rational coordination between the controller different components is essential to ensure efficient control actions. For this purpose, a hybrid structure of fuzzy PD with cascade PI-PD controller (FPD/PI-PD) is proposed for a particular application of the secondary LFC in two interconnected microgrids. In addition to the controller structure, choice of a suitable heuristic technique is crucial for fine-tuning the considered controller to function successfully. Therefore, developing and implementing novel heuristic algorithms will have a substantial contribution to boosting the efficiency of the hybrid control scheme. Recently, a novel heuristic technique called JAYA algorithm (Rao 2016) is introduced. This algorithm has shown excellent feasibility to solve engineering optimization problems (Rao and Saroj 2017; Singh et al. 2017) since it is free from any algorithm parameter settings. In present work, an improved JAYA algorithm called IJAYA is introduced and, subsequently, established to simultaneously tune the decisive coefficients of the proposed controller. The superiority of the FPD/PI-PD controller is verified in a simulation study with other conventional PID and FPID controllers. Finally, the applicability and efficacy of the proposed controller are appraised in real-time platform using the hardware-in-the-loop (HiL) simulation.

2 Case study system and modeling

Figure 1 depicts an isolated MG in which DGs such as PVs and WTGs, and energy storage units such as BESS and FESS supply the distributed loads (Khooban et al. 2016a). The power grid and the MG operation are controlled by the distribution management system (DMS) and the MG dispatch system (MGDS), respectively. Also, the bidirectional information transfer can be achieved through communication links (Yang et al. 2015).

In this study, secondary LFC in the context of MMG is considered which consists of two MGs connected by tie-lines (Chowdhury and Asaduz-Zaman 2014). Each of the MGs is made up of different components, namely synchronous generator (SG), photovoltaic (PV), wind turbine (WT), storage energy systems such as BESS and FESS. A simplified schematic of the concerned MMG is depicted in Fig. 2. As shown in Fig. 2, the frequency deviation is used for regulating the output of BESS and FESS. This control strategy obviates the necessity of establishing a controller for each of the storage components in the feedback path as reported in Das et al. (2012). The parameter values associated with the case study are summarized in Table 1.
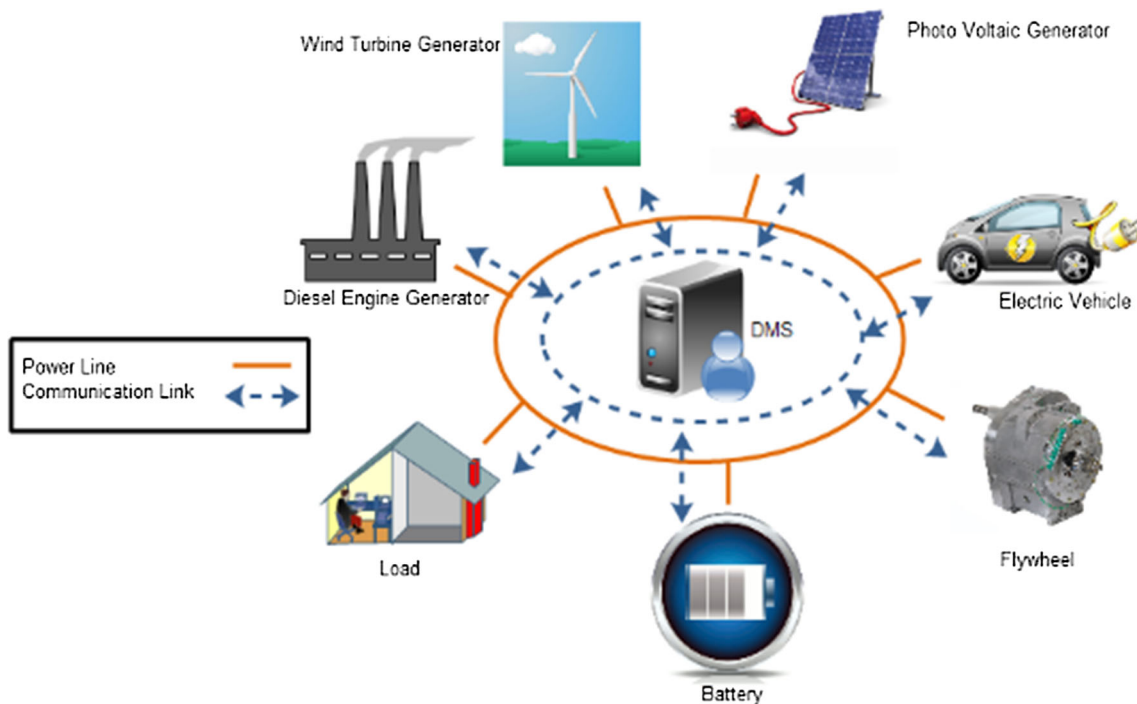
Fig. 1 The general scheme of Microgrids

2.1 Power generation unit

Synchronous generator (SG) can detect the demand variations and regulate its fuel consumption by applying an appropriate control mechanism in an MG environment. The model used for SG in the present work comprises of governor and turbine, which are simplified by first-order plants (Chowdhury and Asaduz-Zaman 2014). The transfer function of the governor is expressed as:

$$G_G = \frac{1}{1 + sT_g} \tag{1}$$

The turbine is described by the below transfer function:

$$G_T = \frac{1}{1 + sT_t} \tag{2}$$

2.2 Wind turbine model

The power generated by WT depends on different factors such as the inherent characteristics of the turbine and wind velocity. The output power of turbine is defined as shown in (3) (Pandey et al. 2014).

$$P_{WT} = \frac{1}{2} A \rho C_p V^3 \tag{3}$$

where A is swept area of rotor blades (m^2), ρ is air density (kg/m3), C_p is power coefficient and V is wind speed.

By neglecting the nonlinearities, the transfer function of WT can be modeled as stated in (4).

$$G_{WT} = \frac{K_{WT}}{1 + sT_{WT}} \tag{4}$$

2.3 Photovoltaic system Model

A solar PV system, made up from many cells, can be implemented as DG microsource in an MG through converting the infinite and inexhaustible solar energy to electrical energy. The amount of power produced by the PV system depends on the surface area of the cell, radiation intensity and ambient temperature. The power taken away from the PV system is calculated as shown in (5) (Chowdhury and Asaduz-Zaman 2014; Das et al. 2012).

$$P_{PV} = \gamma S \varphi [1 - 0.005(T_a + 25)] \tag{5}$$

where γ is the conversion efficiency, S is the PV array area (m^2), φ represents the solar irradiation (KW/m^2) and T_a is ambient temperature.

The transfer function of the PV system can be simplified as a first-order lag:

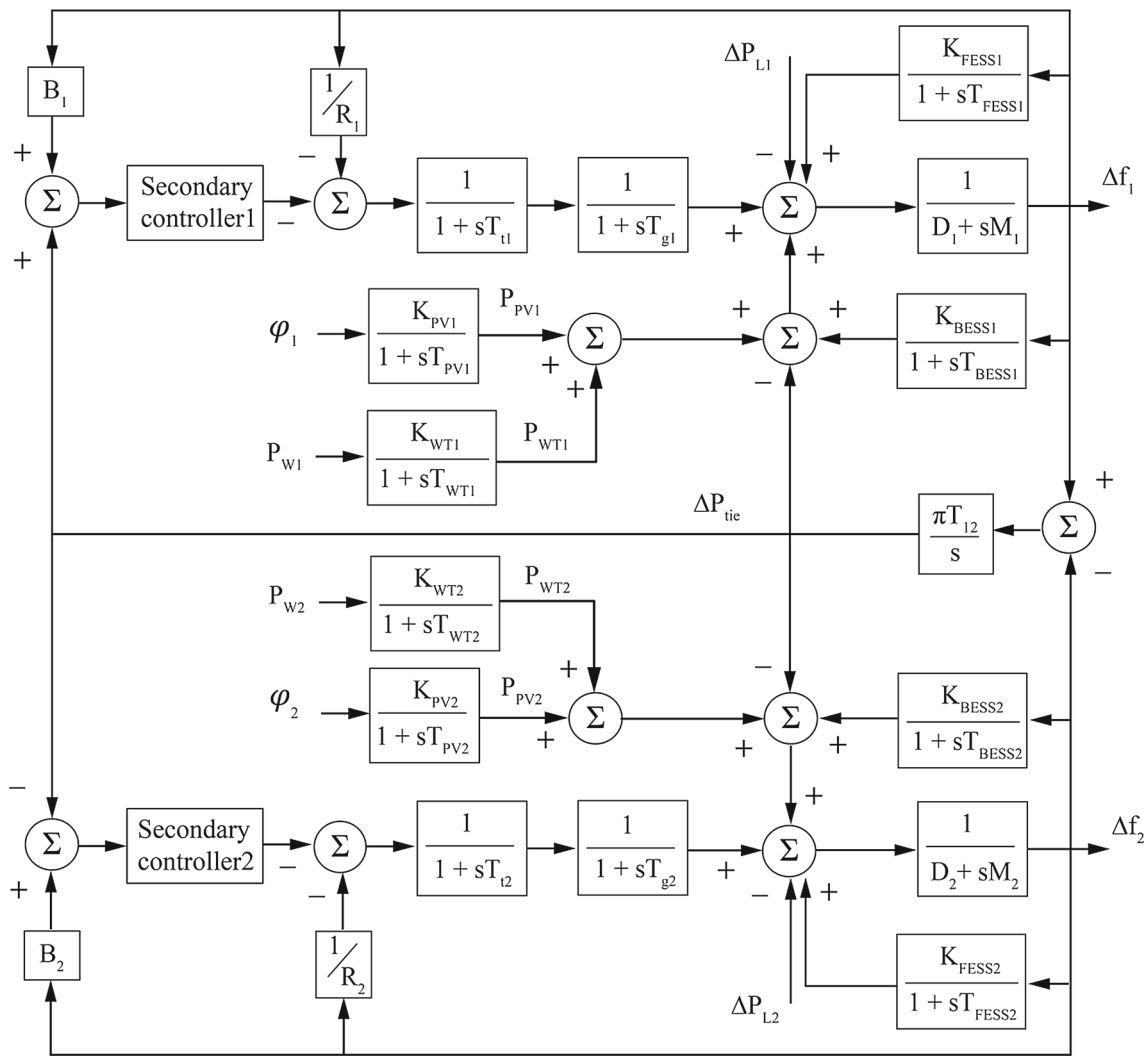$$G_{PV} = \frac{K_{PV}}{1 + sT_{PV}} \tag{6}$$

Fig. 2 Transfer function model of two interconnected microgrid plant

2.4 Energy storage system

Owing to the intermittent specifications of RESs by their nature, BESS and FESS are typically used to prevent the power supply interruptions in an MG. Thus, the energy storage systems play a major role in the reliable operation of MG. The transfer function of BESS and FESS is expressed as given in (7) and (8), respectively (Das et al. 2012).

$$G_{BESS} = \frac{K_{BESS}}{1 + s T_{BESS}} \tag{7}$$

$$G_{FESS} = \frac{K_{FESS}}{1 + s T_{FESS}} \tag{8}$$

3 Controller structure and objective function

3.1 Fuzzy PID controller structure

The fuzzy logic controller (FLC) provides superior applicability to the conventional PID controller. In fact, the FLC establishes a static nonlinearity between its input and output scaling factors (SFs) which enhance the robustness and the overall performance of a closed loop system. Figure 3 (Mohanty et al. 2016) shows a typical configuration of fuzzy PID (FPID) controller which is constructed from fuzzy PI and fuzzy PD controllers. In the given structure, K_1, K_2 are the input SFs and K_P, K_I and K_D are the output SFs.

3.2 Hybrid fuzzy PD and PI-PD controller structure

The control structures of the FLC and cascade PI-PD separately have shown excellent performance over conventional

Table 1 Nominal values of the investigated MMG

System Parameters	Description	MG-1	MG-2
R	Speed regulation constant (p.u.)	0.05	0.04
B	Frequency bias constant (p.u.)	10	12.5
T_t	Time constant of turbine (s)	0.4	0.4
T_g	Speed governor time constant (s)	0.1	0.1
T_{WT}	Time constant of WT (s)	0.5	0.5
T_{PV}	Time constant of PV (s)	1.5	1.5
T_{BESS}	Time constant of BESS (s)	0.1	0.1
T_{FESS}	Time constant of FESS (s)	0.1	0.1
K_T	Turbine gain constant (p.u.)	1	1
K_g	Governor gain constant (p.u.)	1	1
K_{BESS}	Gain constant of BESS (p.u.)	-3	-4
K_{FESS}	Gain constant of FESS (p.u.)	-1.5	-2
K_{WT}	Gain constant of WT (p.u.)	1	1
K_{PV}	Gain constant of PV (p.u.)	1	1
M	Inertia constant (p.u.)	8	8
D	Damping constant (p.u.)	1	1
T_{12}	Synchronizing coefficient	1.4	

PID structured controllers in many applications as reported in the literature (Sahu et al. 2016; Padhy and Panda 2017). To obtain the beneficial sides of both categories with the aim of achieving greater flexibility and resistance, a hybrid configuration of fuzzy PD and cascade PI-PD (FPD/PI-PD)

controllers is suggested in this study. The schematic diagram of the proposed controller structure is depicted in Fig. 4 where K_1 and K_2 are the input SFs of the FLC and K_{P1}, K_I, K_{P2} and K_D are the terms of cascade PI-PD part. In the hybrid structure, the output of FPD controller is the input to PI-PD controller. The output of PI-PD controller is the input signal for the plant to be controlled.

The fixed rule base is chosen for the FLC as tabulated in Table 2, where the acronyms NL, NS, ZR, PS and PL represent the linguistic variables such as negative large, negative small, zero, positive small and positive large, respectively. The relevant membership functions (MFs) are illustrated in Fig. 5 (Sahu et al. 2016).

3.3 Design of objective function

The present work is concentrating on the optimal set of the secondary controller parameters for the studied MMG model. For this purpose, an objective function is defined and then formulated so that settles down the response oscillations to steady value with minimum settling time and minimum overshoot. To meet the considered control objective, integral time absolute error (ITAE) is chosen for assessing the worth of a solution in the optimization algorithm. The expression for the ITAE criterion is stated in (9) (El-Fergany and El-Hameed 2017).
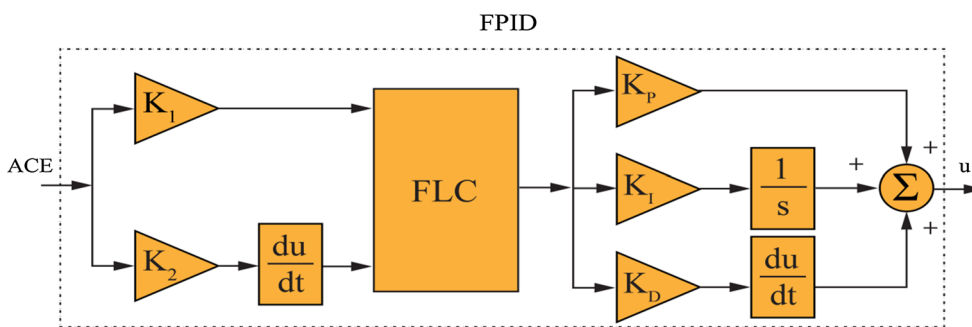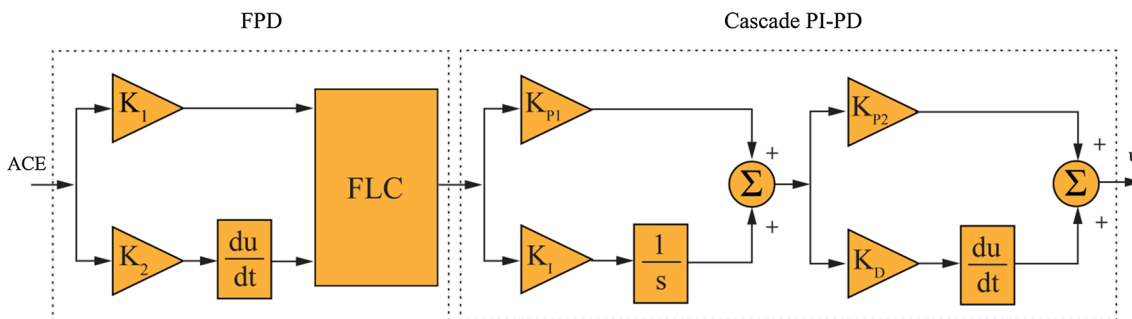

Fig. 3 Structure of FPID controller

Fig. 4 Structure of FPD/PI-PD controller

Table 2 Rule base for the error, derivative of error and FLC output

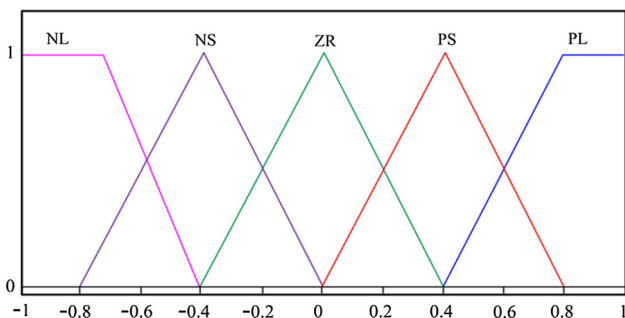| ACE	ΔACE				
	NL	NS	Z	PS	PL
NL	NL	NL	NL	NS	Z
NS	NL	NL	NS	Z	PS
Z	NL	NS	ZR	PS	PB
PS	NS	ZR	PS	PB	PB
PL	ZR	PS	PB	PB	PB

Fig. 5 Membership functions for error, derivative error and FLC output

$$J = \text{ITAE} = \int_0^{t_{sim}} (|\Delta f_1| + |\Delta f_2| + |\Delta P_{tie}|).t.dt \qquad (9)$$

where t_{sim} is the final time of simulation.

4 JAYA algorithm

The JAYA algorithm is a simple and potent algorithm which is recently developed by Rao (2016). In the algorithm, the individuals try to improve their position by moving toward the best solution and avoiding the worst solution simultaneously.

At the beginning of the JAYA algorithm, a set of candidate solutions is randomly initialized with the size P (i.e., $i = 1, 2, \ldots, P$) and each solution $y_j = (y_1, y_2, \ldots, y_D)$ is a D-dimensional vector. A new solution is then determined by the following equation.

$$Y_{i,j}^k = y_{i,j}^k + \text{rand}_1 \left(y_{j,\text{best}}^k - |y_{i,j}^k| \right)$$
$$- \text{rand}_2 \left(y_{j,\text{worst}}^k - |y_{i,j}^k| \right) \qquad (10)$$

where $Y_{i,j}^k$ is the updated solution of $y_{i,j}^k$ during kth iteration; rand_1 and rand_2 are uniform random numbers in [0 1]; $y_{j,\text{best}}^k$ and $y_{j,\text{worst}}^k$ are the best and worst values obtained until the kth iteration. The modified solutions are considered as input to the next generation if its fitness value is better than the old solution. The pseudo-code for the JAYA approach is given in Algorithm 1.

Algorithm 1: The pseudo-code of the JAYA algorithm.

```
Initialize the parameters Max-Gen, P and D
for i=1 to P do
    for j=1 to D
        y_{i,j} = lb_j + rand * (ub_j − lb_j);
    end for
end for
    while gen=1 to Max-Gen do
        for i=1 to P do
            Identify the best and worst solutions in the population
            Update the solutions by the Eq. (10)
        end for
Check limitations and repair the solutions if they are violated from
boundary constraints
        for i=1 to P do
            if f(Y_i) < f(y_i) then
                Replace y_i with Y_i
            end if
        end for
        Report the optimum solution
    end while
```

5 Improved JAYA algorithm

5.1 Chaotic extended opposition-based initialization

Initialization phase plays a vital role in the performance of heuristic algorithms in terms of the convergence characteristic and the quality of the final solution. Based on the idea that the opposite point of a solution may be close to the global optimum, the theory of opposition-based learning (OBL) was introduced by Tizhoosh (2005). Literature (Xiang et al. 2014) reports that the take advantage of OBL will enhance the diversity and suitability of initial population. In this regard, a chaotic extended opposition is applied here for the efficient initialization of input parameters of JAYA algorithm.

Extended opposition (Seif and Ahmadi 2015) generates a random number within the opposition point of a solution and the nearest bound to its opposite number, which is defined as the expression characterized in (11).

$$\check{y}_{j,eo} = \begin{cases} \text{rand}(\check{y}_j, \text{ub}_j), & y_j < (\text{lb}_j + \text{ub}_j)/2 \\ \text{rand}(\text{lb}_j, \check{y}_j), & y_j > (\text{lb}_j + \text{ub}_j)/2 \end{cases} \qquad (11)$$

where $j = 1, 2, \ldots, D$; lb_j and ub_j are the lower and upper bound for each component j, respectively. $\check{y}_{eo}$ represents the extended opposite point of y, and $\check{y}$ is the opposite point of y where $\check{y}_j = \text{lb}_j + \text{ub}_j - y_j$.

To further enrich the initialization based on the extended opposition, chaotic sequences are adopted to diversify the candidate solutions in space interval, instead of random distribution. In the current study, the well-known logistic

equation is chosen and the equation is described in (12) (Secui 2015).

$$x^k = 4x^{k-1}(1 - x^{k-1}) \tag{12}$$

where x^k is the kth chaotic number that is distributed in the range [0 1], while x^0 must not be 0, 0.25, 0.5, 0.75 or 1.

To incorporate the chaotic extended opposition into the population initialization, the solutions y and $\check{y}_{eo}$ are merged and the P fittest solutions are selected as an initial population of JAYA.

5.2 Enhanced global searching-based firefly algorithm

According to the strategy employed in JAYA algorithm, the diversity of solutions depends on the distance between best and worst individuals. As a major lack of this scheme, the solutions will lose their diversity when converges to the goal point in final generations. This situation leads to the iterative process search the decisive space in a small part and, thus increases the risk of trapping into a local optimum. To handle this problem and to preserve a right trade-off between diversity and convergence speed, the updating operation in JAYA algorithm is modified by the idea implemented in firefly algorithm (FA) (Yang 2009). In this approach, with a probability 0.5, the solutions are updated by the original JAYA. Otherwise, the solutions are updated as follows:

$$\begin{aligned} Y_{i,j}^k = y_{i,j}^k &+ \mathrm{rand}_1 e^{-r_{\mathrm{gx}}^2} \left(y_{j,\mathrm{best}}^k - |y_{i,j}^k| \right) \\ &- \mathrm{rand}_2 e^{-r_{\mathrm{wx}}^2} \left(y_{j,\mathrm{worst}}^k - |y_{i,j}^k| \right) \\ &+ \alpha(\psi - 1/2) \end{aligned} \tag{13}$$

where α is a user-supplied scaling factor, ψ is a random number in [0 1], r_{gx} and r_{wx} are the euclidean distance between $\{y_{i,j}, y_{j,\mathrm{best}}^k\}$, $\{y_{i,j}, y_{j,\mathrm{worst}}^k\}$ as stated in (14) and (15), respectively.

$$r_{\mathrm{gx}} = \sqrt{\sum_{j=1}^{D} (y_{j,\mathrm{best}} - y_{i,j})^2} \tag{14}$$

$$r_{\mathrm{wx}} = \sqrt{\sum_{j=1}^{D} (y_{j,\mathrm{worst}} - y_{i,j})^2} \tag{15}$$

The computational procedure of the proposed IJAYA technique is illustrated in Algorithm 2.

Fig. 6 The real-time experimental setup

6 Simulation results

In this section, the efficiency of the IJAYA-based FPD/PI-PD controller, by employing ITAE criterion, is evaluated to deal with the LFC issue of MMG as presented in Fig. 2. Distinct secondary regulators are established for each MG, and the closed loop system is examined against various scenarios of step variation and stochastic fluctuation in load and RESs (wind and solar). Conventional controller structures such as PID and FPID controllers are also designed and applied to the concerned MMG for the comparison purposes. The lower and upper limitations are taken as 0 and 3 for all the gains and scaling factors of the different controllers, and the simulation time of $t_{\mathrm{sim}} = 120\mathrm{s}$ is considered in this investigation. Besides, this paper has tried to do all simulation results by the OPAL-RT to validate the possibility of the practical implementation of the proposed method. The real-time simulator (RTS) works as a parallel computation, which leads to carry out complex computations with very amazing accuracy as well as low-cost real-time implementation. The hardware-in-the-loop (HIL) trials are accomplished essentially for two objectives. Firstly, to prove the effectiveness and correctness of the suggested controller in actual multi-MGs. Secondly, to assess the real-time computing ability, accuracy, performance and robustness of the proposed

Table 3 Step variation of load, wind turbine output and sun irradiance

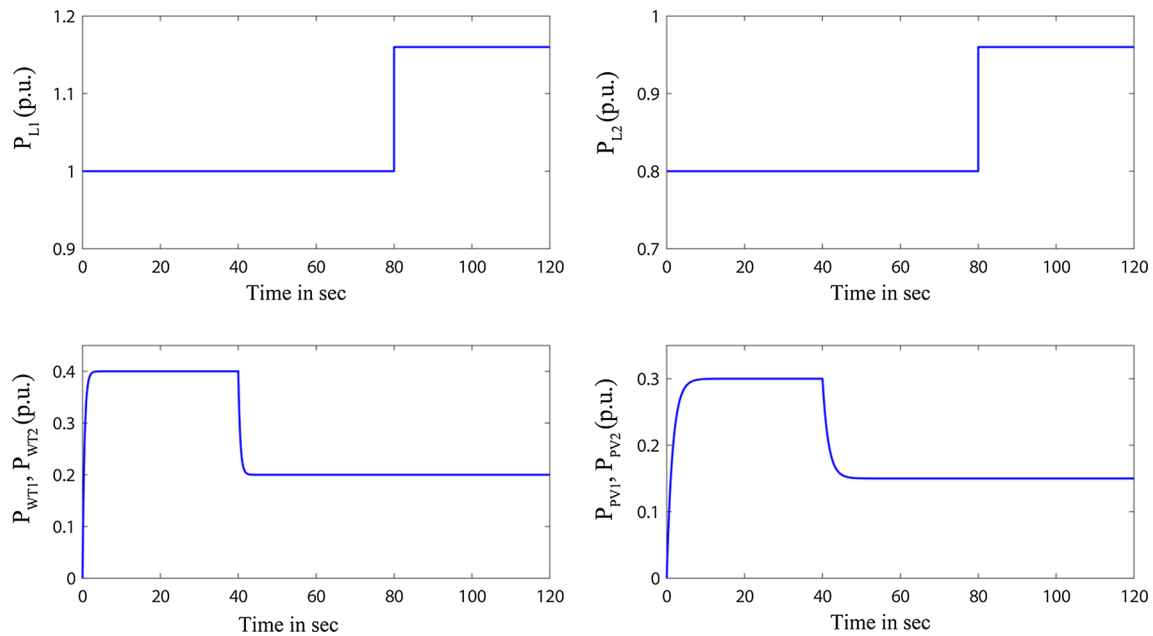| Disturbances at	Range
Load in MG-1	$0 < t < 80$: 1 p.u.
	$80 < t < 120$: 1.16 p.u.
Load in MG-2	$0 < t < 80$: 0.8 p.u.
	$80 < t < 120$: 0.96 p.u.
Wind turbine	$0 < t < 40$: 0.4 p.u.
	$40 < t < 120$: 0.2 p.u.
Sun irradiance	$0 < t < 40$: 0.3 p.u.
	$40 < t < 120$: 0.15 p.u.

Fig. 7 A step change of load demand and power generated from WT and PV

Table 4 Optimal controller parameters and minimum fitness value for step-type disturbances

| Controller parameters/fitness value	GA: PID	Jaya: PID	IJaya: PID	IJaya: FPID	IJaya:FPD/PI-PD
MG-1	$K_P = 2.7143$	$K_P = 1.8498$	$K_P = 2.8779$	$K_1 = 2.9315$	$K_1 = 2.9676$
	$K_I = 3.0000$	$K_I = 3.0000$	$K_I = 3.0000$	$K_2 = 0.0011$	$K_2 = 0.7349$
	$K_D = 1.8664$	$K_D = 0.9657$	$K_D = 0.5739$	$K_P = 2.7184$	$K_{P1} = 0.0527$
				$K_I = 2.8868$	$K_I = 2.9996$
				$K_D = 0.9392$	$K_{P2} = 3.0000$
					$K_D = 2.2957$
MG-2	$K_P = 1.7822$	$K_P = 1.0135$	$K_P = 1.8406$	$K_1 = 2.4643$	$K_1 = 2.9417$
	$K_I = 2.3317$	$K_I = 2.4160$	$K_I = 2.4149$	$K_2 = 0.0348$	$K_2 = 0.0988$
	$K_D = 1.6924$	$K_D = 0.7498$	$K_D = 0.4377$	$K_P = 2.8078$	$K_{P1} = 2.6059$
				$K_I = 2.8473$	$K_I = 2.9641$
				$K_D = 1.0899$	$K_{P2} = 2.3570$
					$K_D = 0.4270$
ITAE	2.5021	2.0892	2.0444	0.5735	0.2233
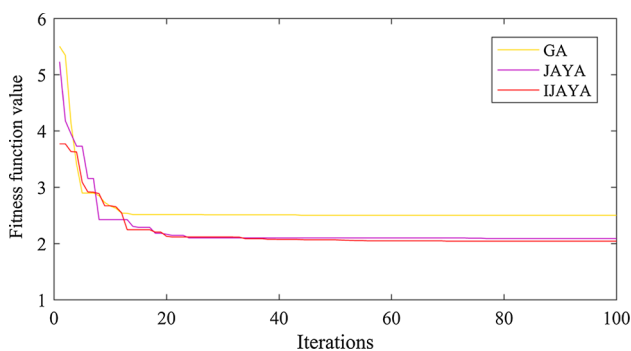
Fig. 8 Convergence characteristics for various algorithms with PID controller

method in the real world. Besides, the RTS based on OPAL-RT technology is utilized to simulate errors and delays which do not exist in the classical off-line simulations. Figure 6 sketches the HIL setup, consisting of: 1) OPAL-RT as a real-time simulator (RTS) which simulates the MG depicted in Fig. 2; 2) a PC as the command station (programming host) in which the Matlab/Simulink-based code that is executed on the OPAL-RT is generated; and 3) a router used as a connector of all the setup devices in the same sub-network. The OPAL-RT is also connected to the DK60 board through Ethernet ports. More details about the components of this setup can be found in Khooban et al. (2017a, b), Khooban (2017)

Algorithm 2: The pseudo-code of the proposed IJAYA algorithm.

Initialize the parameters Max-Gen, P, D and α
for i=1 to P **do**
    for j=1 to D
        $y_{i,j} = lb_j + rand * (ub_j - lb_j)$;
    end for
end for
for i=1 to P **do**
    for j=1 to D **do**
        $C_{i,j} = (lb_j + ub_j)/2$;
        Randomly initialize chaos variables $x_j^0 \epsilon (0\ 1)$
        if $(y_{i,j} < C_{i,j})$ **then**
        $\breve{y}_{i,j}^{eo} = \breve{y}_{i,j} + 4 x_j^{k-1}(1 - x_j^{k-1})(ub_j - \breve{y}_{i,j})$;
        else
        $\breve{y}_{i,j}^{eo} = lb_j + 4 x_j^{k-1}(1 - x_j^{k-1})(\breve{y}_{i,j} - lb_j)$;
        end if
    end for
end for
Select P fittest individuals from set of $\{y_{i,j}, \breve{y}_{i,j}^{eo}\}$ as the initial population.
  while gen=1 to Max-Gen **do**
    for i=1 to P **do**
     Identify the best and worst solutions in the population
     if rand < 1/2 **then**
     Update the solutions by the original JAYA algorithm
      else
     Calculate r_{gx} and r_{wx} using Eqs. (14) and (15)
     Update the solutions by the Eq. (13)
     end if
    end for
Check limitations and repair the solutions if they are violated from boundary constraints
    for i=1 to P **do**
      if $f(Y_i) < f(y_i)$ **then**
       Replace y_i with Y_i
      end if
    end for
    Report the optimum solution
  end while

Case 1:

In the first instance, step changes in load, wind and sun irradiance are considered which are given in Table 3. The load demand (P_L), the power output of wind turbine (P_{WT}) and solar photovoltaic (P_{PV}) are depicted in Fig. 7. To explore the efficiency of the proposed IJAYA algorithm and to perform a more visible comparison analysis, primarily, PID controller is regulated employing GA, JAYA and IJAYA. The control parameters for execution of these algorithms are available in "Appendix (A.1)–(A.3)." It is noted that the algorithms are over 30 times repeated and the best final solutions are chosen as controller parameters. The tuned parameters and the computed ITAE values with the application of the concerned step disturbances are offered in Table 4. The convergence profiles for different algorithms-based PID controller are presented in Fig. 8. As viewed in Fig. 8, IJAYA outperforms GA and JAYA with the better computational capability and global exploration without any undesirable oscillations.

Then, the existing results are further improved through adopting IJAYA-based FPID and FPD/PI-PD controllers. The optimal settings of the controllers are also available in Table 4. A minimization of ITAE value is obtained by
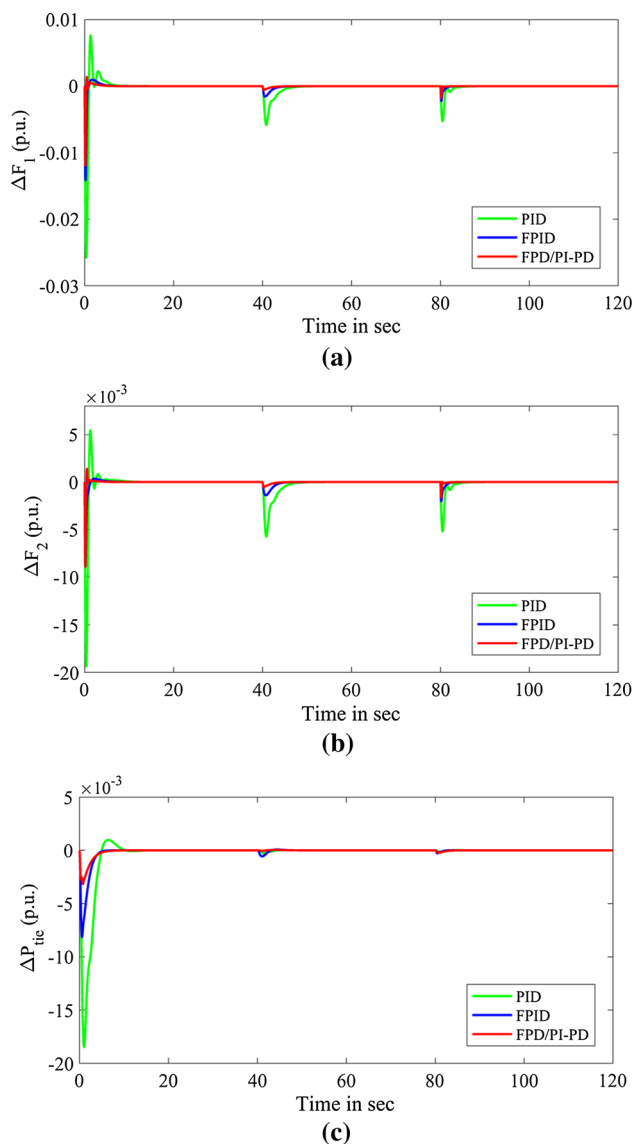

Fig. 9 Comparative transient responses for step-type disturbances. **a** Frequency deviation in MG-1, **b** Frequency deviation in MG-2, **c** Tie-line power deviation

Table 5 The parameters values for stochastic fluctuations of load, wind turbine and sun irradiance

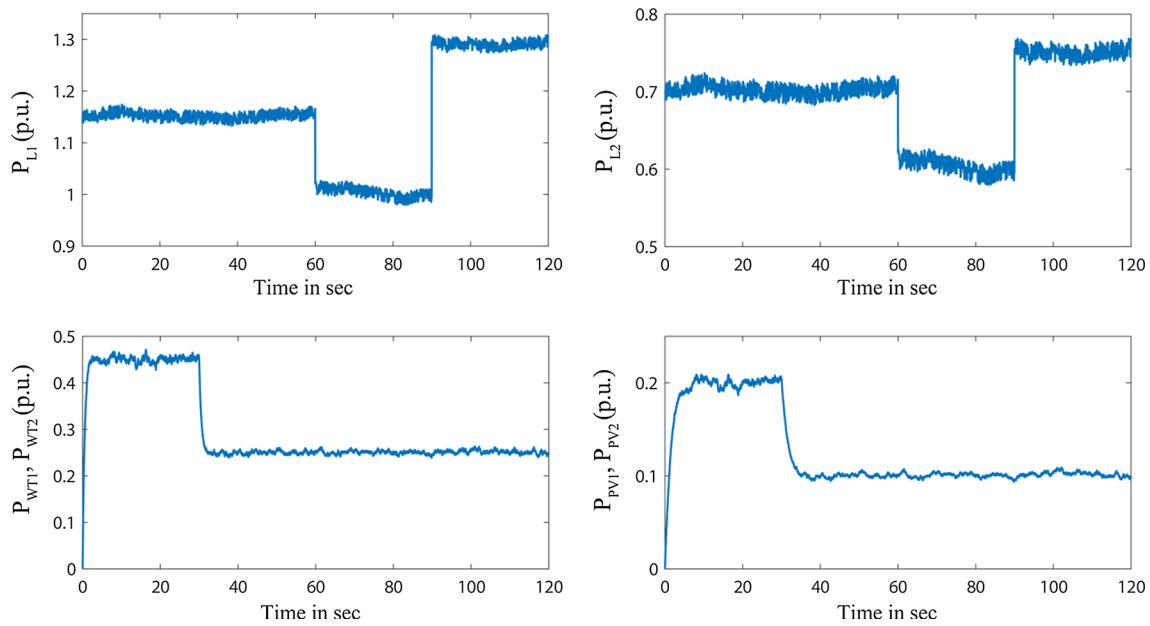| Disturbances at	Parameters			
	ϕ	η	β	$G(s)$
Load in MG-1	$\cup(-1, 1)$	0.8	10	$\frac{300}{(300s+1)} + \frac{1}{(1800s+1)}$
Load in MG-2	$\cup(-1, 1)$	0.8	10	$\frac{300}{(300s+1)} + \frac{1}{(1800s+1)}$
Wind turbine	$\cup(-1, 1)$	0.8	10	$\frac{1}{(10^4 s+1)}$
Sun irradiance	$\cup(-1, 1)$	0.7	1	$\frac{1}{(10^4 s+1)}$

Fig. 10 Stochastic fluctuation of load demand and power generated from WT and PV

proposed IJAYA-based FPD/PI-PD controller than other controller structures. The dynamic responses of IJAYA-based PID, FPID and FPD/PI-PD controllers in terms Δf_1, Δf_2 and ΔP_{tie} are painted in Fig. 9. It is seen in Fig. 9 that the proposed structured controller provides better transient behavior, i.e., improving damping and settling down characteristics, than the comparative structures to handle the aforesaid disturbances.

Case 2:

In this case, for more realistic analysis, small stochastic fluctuations of load demand, wind power and sun irradiance are applied in the MMG model. The template considered in this work to generate the output power P is of the form (16) (Pan and Das 2015).

$$P = (\phi\eta\sqrt{\beta}(1 - G(s)) + \beta)/\beta)\Gamma = \lambda.\Gamma \qquad (16)$$

where ϕ is the stochastic component of the power, η is the normalization constant of generated power (λ), β is the mean value, Γ suddenly switches the level fluctuation power to a defined value at a specific time. The associated parameters used in the simulation are given in Table 5. In this work, the signals of load, wind turbine and photovoltaic are formed as characterized in (17)-(20).

$$\Gamma_{L1} = 0.05H(t) + [1.1H(t) - 0.15H(t-60)$$
$$+ 0.3H(t-90)](1/\lambda) \qquad (17)$$
$$\Gamma_{L2} = 0.05H(t) + [0.65H(t) - 0.10H(t-60)$$
$$+ 0.16H(t-90)](1/\lambda) \qquad (18)$$
$$\Gamma_{WT1} = \Gamma_{WT2} = 0.45H(t) - 0.2H(t-30) \qquad (19)$$

Table 6 Optimal controller parameters and minimum fitness value for stochastic-type disturbances with IJaya technique

Controller parameters/fitness value	PID	FPID	FPD/PI-PD
MG-1	$K_P = 3.0000$	$K_1 = 2.995$	$K_1 = 3.0000$
	$K_I = 3.0000$	$K_2 = 2.3072$	$K_2 = 2.4330$
	$K_D = 1.0975$	$K_P = 2.9892$	$K_{P1} = 0.0407$
		$K_I = 3.0000$	$K_1 = 2.9999$
		$K_D = 0.0013$	$K_{P2} = 2.9942$
			$K_D = 2.8610$
MG-2	$K_P = 1.8808$	$K_1 = 2.7031$	$K_1 = 2.9989$
	$K_I = 2.4012$	$K_2 = 2.8073$	$K_2 = 3.0000$
	$K_D = 0.8280$	$K_P = 2.4464$	$K_{P1} = 2.3579$
		$K_I = 2.4970$	$K_1 = 3.0000$
		$K_D = 0.0143$	$K_{P2} = 2.5775$
			$K_D = 0.0277$
ITAE	8.2751	2.7823	1.1712

$$\Gamma_{PV1} = \Gamma_{PV2} = 0.2H(t) - 0.1H(t-30) \qquad (20)$$

where H(t) represents Heaviside step function. The relevant profiles of P_{L1}, P_{L2}, P_{WT} and P_{PV} are depicted in Fig. 10. The stochastic fluctuations in Fig. 10 are applied to the studied MMG, and the IJAYA algorithm is executed for optimal computation of the gains and SFs of PID, FPID and FPD/PI-PD controllers. The regulated controller parameters and minimum ITAE value are arranged in Table 6. The profiles of the frequency and tie-line power deviations corresponding to the
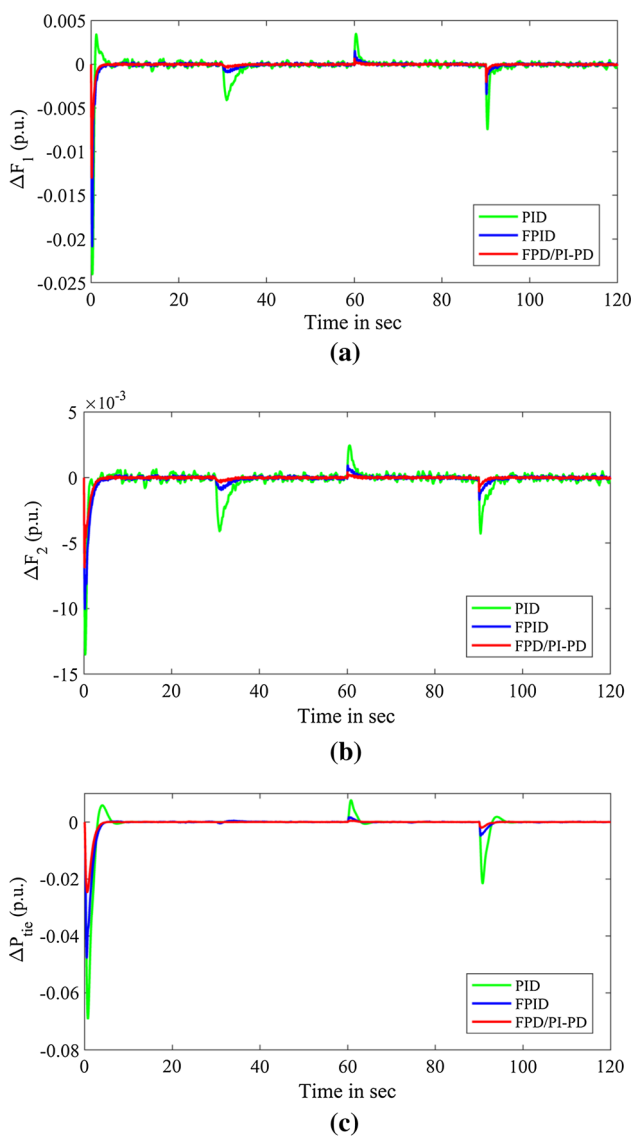
Fig. 11 Comparative transient responses for stochastic-type disturbances. **a** Change of frequency in MG-1, **b** Change of frequency in MG-2, **c** Change of tie-line power

Fig. 12 The output power of storage energy systems. **a** The output power of BESS in MG-1, **b** The output power of FESS in MG-1

Table 7 Parameter variations of the MMG

Parameters	Scenario 1 (%) (%	Scenario 2 (%)	Scenario 3 (%)
T_g	-20	-45	-75
T_t	$+25$	$+50$	$+58$
B	-30	-53	-63
R	$+30$	$+35$	$+60$
D	-22	-40	-70
M	$+30$	$+55$	$+60$
T_{BESS}	-25	-50	-75
T_{FESS}	30	$+40$	$+65$

designed controllers are painted in Fig. 11. As visualized in Fig. 11, the transient responses of FPD/PI-PD controller are much smoother and the overshoots are smaller than the other two controllers.

The power generated by energy storage systems (BESS and FESS) equipped in the feedback path is illustrated in Fig. 12. It is evident that with the proposed structure of FPD/PI-PD controller, the system is faster to quickly alleviate the response oscillations in comparison with PID and FPID controllers. Thus, the smaller size of the energy storage systems can be adopted by the proposed controller structure. This is a valuable contribution to the efficiency of MMG from the health and economics point of the view.
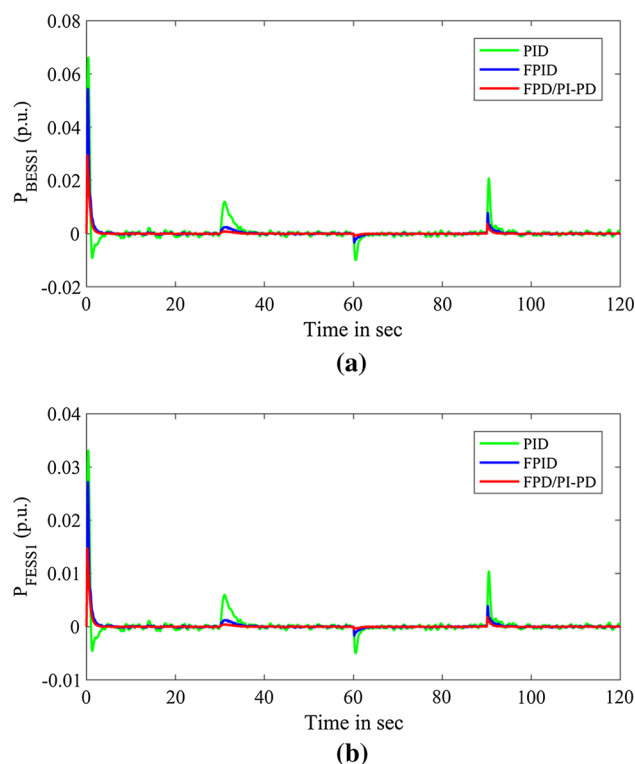
Case 3:

A parametric variation analysis is conducted for the Case 2 to evaluate the robustness of the regulated PID, FPID and FPD/PI-PD controllers-based LFC of MMG. The associated tuned parameters of the controllers offered in Table 6 are examined by varying some system parameters by three individual scenarios as presented in Table 7. The profiles of frequency deviation in the MG-1 for all the scenarios are plotted in Fig. 13. The performance measure (ITAE) values calculated for the various controllers are depicted in Fig. 14. Critical observation of Fig. 13 and Fig. 14 reveals that there is an insignificant effect on the performance of FPD/PI-PD with the different scenarios. It is also evident that the gains of PID controller have not adequate flexibil-
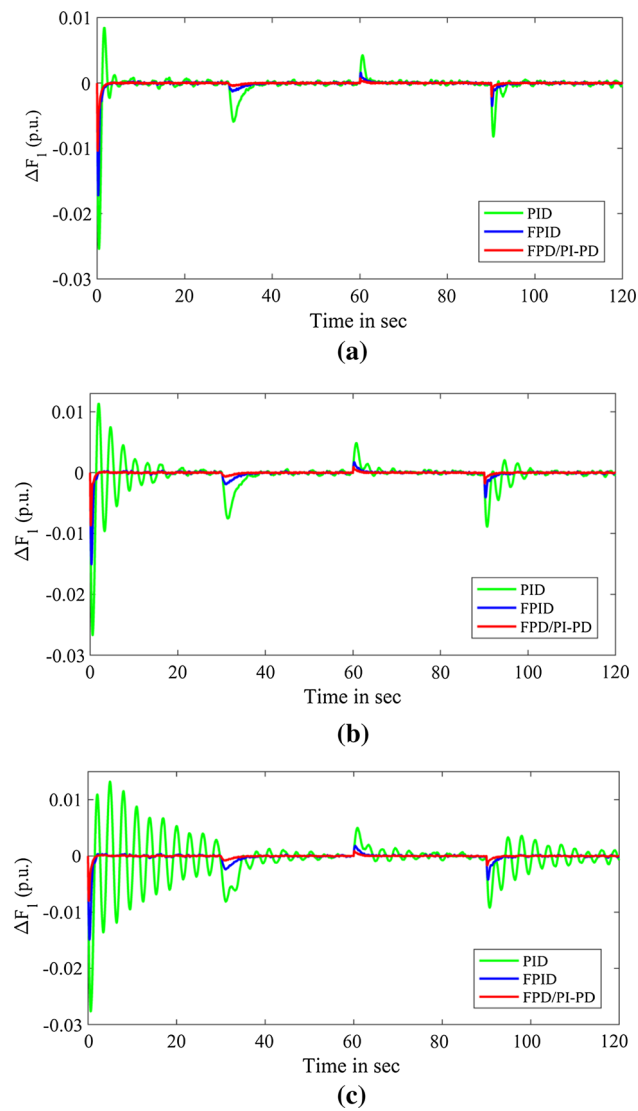
Fig. 14 Computed ITAE in different uncertain conditions

7 Conclusion

In this article, an attempt is conducted to heighten the dynamic stability of an LFC of a multi-microgrid system employing a fuzzy PD-based cascade PI-PD controller (FPD/PI-PD controller). For the optimal design of the controller parameters, a novel variant of JAYA algorithm is proposed with improved initialization diversification and enhanced global searching ability characteristics than the original JAYA algorithm. The proposed technique was applied in a way that handles the stochastic load disturbances and the effect of the power fluctuations caused by the variations of the wind speed and sun irradance. The simulation results confirm that IJAYA outperforms GA and JAYA. Also, it was proved that when the fuzzy PD controller is combined in series with PI-PD controller, the dynamic behavior of the system is remarkably improved as compared with the conventional PID and FPID structured controllers.

Compliance with ethical standards

Conflict of interest Both authors declare that they have no conflict of interest.

Research involving human participants and/or animals This article does not contain any studies with human participants or animals performed by any of the authors.

Informed consent This article does not contain any studies with human participants or animals performed by any of the authors.

Fig. 13 Comparative dynamic responses with stochastic disturbances and parametric variations. **a** Change in frequency of MG-1 according to scenario 1. **b** Change in frequency of MG-1 according to scenario 2. **c** Change in frequency of MG-1 according to scenario 3

ity against the robustness testing (especially scenario 3) and the system response experiences large fluctuations. Hence, it can be concluded that PID controllers are unable to control the MMG when the system is subjected to sever parameter variations. Also, the time domain simulation proves that the performance of hybrid structure of FLC and PID controllers (FPID and FPD/PI-PD) is independent of retuning controller parameters; however, proposed control structure provides a higher degree of robustness against the aforesaid parameter perturbations.
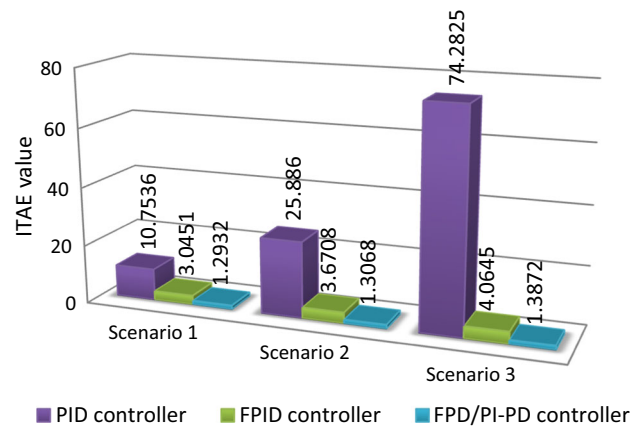
Appendix A

A.1) Genetic parameters: P=20; Max-Gen=100; crossover probabilities=0.85; mutation probabilities=0.1.
A.2) JAYA parameters: P=20; Max-Gen=100.
A.3) IJAYA parameters: P=20; Max-Gen=100, $\alpha = 0.4$.

Appendix B - Symbols

R	Speed regulation constant (p.u.)
B	Frequency bias constant (p.u.)
T_t	Time constant of turbine (s)
T_g	Speed governor time constant (s)
T_{WT}	Time constant of WT (s)
T_{PV}	Time constant of PV (s)
T_{BESS}	Time constant of BESS (s)
T_{FESS}	Time constant of FESS (s)
K_T	Turbine gain constant (p.u.)
K_g	Governor gain constant (p.u.)
K_{BESS}	Gain constant of BESS (p.u.)
K_{FESS}	Gain constant of FESS (p.u.)
K_{WT}	Gain constant of WT (p.u.)
K_{PV}	Gain constant of PV (p.u.)
M	Inertia constant (p.u.)
D	Damping constant (p.u.)
T_{12}	Synchronizing coefficient

References

Bajpai P, Dash V (2012) Hybrid renewable energy systems for power generation in stand-alone applications: a review. Renew Sustain Energy Rev 16:2926–2939

Bevrani H, Habibi F, Babahajyani P, Watanabe M, Mitani Y (2012) Intelligent frequency control in an AC microgrid: online PSO-based fuzzy tuning approach. IEEE Trans Smart Grid 3:1935–1944

Chowdhury AH, Asaduz-Zaman M (2014) Load frequency control of multi-microgrid using energy storage system. In: IEEE international conference electrical computing enginerring (ICECE) pp 548–551

Chowdhury S, Crossley P (2009) Microgrids and active distribution networks, The Institution of Engineering and Technology

Das DC, Roy AK, Sinha N (2012) GA based frequency controller for solar thermal-diesel-wind hybrid energy generation/energy storage system. Int J Electr Power Energy Syst 43:262–279

El-Fergany AA, El-Hameed MA (2017) Efficient frequency controllers for autonomous two-area hybrid microgrid system using social-spider optimiser. IET Gener Trans Distrib 11:637–648

Goya T, Omine E, Kinjyo Y, Senjyu T, Yona A, Urasaki N, Funabashi T (2011) Frequency control in isoalated island by using parallel operated battery systems applying H∞ control theory based on droop characteristics. IET Renew Power Gener 5:160–166

Kargarian A, Rahmani M (2015) Multi-microgrid energy systems operation incorporating distribution-interline power flow controller. Electr Power Syst Res 129:208–216

Khalghani MR, Khooban MH, Mahboubi-Moghaddam E, Vafamand N, Goodarzi M (2016) A self-tuning load frequency control strategy for microgrids: human brain emotional learning. Int J Elect. Power Energy Syst 75:311–319

Khooban MH (2017) Secondary load frequency control of time-delay stand-alone microgrids with electric vehicles. IEEE Trans Ind Electr. https://doi.org/10.1109/TIE.2017.2784385

Khooban MH, Niknam T (2015) A new intelligent online fuzzy tuning approach for multi-area load frequency control: self adaptive modified bat algorithm. Int J Electr Power Energy Syst 71:254–261. https://doi.org/10.1016/j.ijepes.2015.03.017

Khooban M-H, Niknam T, Blaabjerg F, Davari P, Dragicevic T (2016a) A robust adaptive load frequency control for micro-grids. ISA Trans 65:220–229

Khooban MH, ShaSadeghi M, Niknam T, Blaabjerg F (2016b) Analysis, control and design of speed control of electric vehicles delayed model: multi-objective fuzzy fractional-order PI λ D μ controller. IET Sci Meas Technol 11:249–261

Khooban M-H, Niknam T, Shasadeghi M, Dragicevic T, Blaabjerg F (2017a) Load frequency control in microgrids based on a stochastic non-integer controller. IEEE Trans Sustain Energy. https://doi.org/10.1109/TSTE.2017.2763607

Khooban M-H, Dragovich T, Blaabjerg F, Delimar M (2017b) Shipboard microgrids: a novel approach to load frequency control. IEEE Trans Sustain Energy. https://doi.org/10.1109/TSTE.2017.2763605

Khooban MH, Niknam T, Blaabjerg F, Dragičević T (2017c) A new load frequency control strategy for micro-grids with considering electrical vehicles. Electr Power Syst Res 143:585–598

Mahto T, Mukherjee V (2016) Evolutionary optimization technique for comparative analysis of different classical controllers for an isolated wind-diesel hybrid power system. Swarm Evol Comput 26:120–136

Modirkhazeni A, Almasi ON, Khooban MH (2016) Improved frequency dynamic in isolated hybrid power system using an intelligent method. Int J Electr Power Energy Syst 78:225–238

Mohanty PK, Sahu BK, Pati TK, Panda S, Kar SK (2016) Design and analysis of fuzzy PID controller with derivative filter for AGC in multi-area interconnected power system. IET Gener Trans Distrib 10:3764–3776

Mukherjee V (2015) A novel quasi-oppositional harmony search algorithm and fuzzy logic controller for frequency stabilization of an isolated hybrid power system. Int J Electr Power Energy Syst 66:247–261

Padhy S, Panda S (2017) A hybrid stochastic fractal search and pattern search technique based cascade PI-PD controller for automatic generation control of multi-source power systems in presence of plug in electric vehicles. CAAI Trans Intell Technol 2:12–25

Pahasa J, Ngamroo I (2016) Coordinated control of wind turbine blade pitch angle and PHEVs using MPCs for load frequency control of microgrid. IEEE Syst J 10:97–105

Pan I, Das S (2015) Kriging based surrogate modeling for fractional order control of microgrids. IEEE Trans Smart Grid 6:36–44

Pandey SK, Mohanty SR, Kishor N, Catalão JPS (2014) Frequency regulation in hybrid power systems using particle swarm optimization and linear matrix inequalities based robust controller design. Int J Electr Power Energy Syst 63:887–900

Rao R (2016) Jaya: a simple and new optimization algorithm for solving constrained and unconstrained optimization problems. Int J Ind Eng Comput 7:19–34

Rao RV, Saroj A (2017) Constrained economic optimization of shell-and-tube heat exchangers using elitist-Jaya algorithm. Energy 128:785–800

Sahu BK, Pati TK, Nayak JR, Panda S, Kar SK (2016) A novel hybrid LUS-TLBO optimized fuzzy-PID controller for load frequency control of multi-source power system. Int J Electr Power Energy Syst 74:58–69

Sa-ngawong N, Ngamroo I (2015) Intelligent photovoltaic farms for robust frequency stabilization in multi-area interconnected power system based on PSO-based optimal Sugeno fuzzy logic control. Renew Energy 74:555–567

Secui DC (2015) The chaotic global best artificial bee colony algorithm for the multi-area economic/emission dispatch. Energy 93:2518–2545

Seif Z, Ahmadi MB (2015) An opposition-based algorithm for function optimization. Eng Appl Artif Intell 37:293–306

Şerban I, Marinescu C (2011) Aggregate load-frequency control of a wind-hydro autonomous microgrid. Renew Energy 36:3345–3354

Singh SP, Prakash T, Singh VP, Babu MG (2017) Analytic hierarchy process based automatic generation control of multi-area interconnected power system using Jaya algorithm. Eng Appl Artif Intell 60:35–44

Tizhoosh HR (2005) Opposition-based learning: a new scheme for machine intelligence. In: IEEE international conference on computational intelligence for modelling, control and automation and international conference on intelligent agents, web technologies and internet commerce (CIMCA-IAWTIC'06) pp 695–701

Torreglosa JP, García P, Fernández LM, Jurado F (2015) Energy dispatching based on predictive controller of an off-grid wind turbine/photovoltaic/hydrogen/battery hybrid system. Renew Energy 74:326–336

Xiang W, An M, Li Y, He R, Zhang J (2014) An improved global-best harmony search algorithm for faster optimization. Expert Syst Appl 41:5788–5803

Yang X-S (2009) Firefly algorithms for multimodal optimization. In: International symposium on stochastic algorithms. Springer, Berlin, pp 169–178

Yang J, Zeng Z, Tang Y, Yan J, He H, Wu Y (2015) Load frequency control in isolated micro-grids with electrical vehicles based on multivariable generalized predictive theory. Energies 8:2145–2164